Smart Rocks and Wireless Communication Systems for Real-Time Monitoring and Mitigation of Bridge Scour
(Progress Report No. 4)

Contract No: RITARS-11-H-MST
(Missouri University of Science and Technology)

Ending Period: June 30, 2012

PI: Genda Chen
Co-PIs: David Pommerenke and Rosa Y. Zheng

Program Manager: Mr. Caesar Singh

Submission Date: July 15, 2012

TABLE OF CONTENTS

EXECUTIVE SUMMARY

In the fourth quarter, the research activities mainly involved the preparation, test and localization of smart rocks in a small flume and a large flume of the Hydraulics Engineering Laboratory at Turner-Fairbank Highway Research Center (TFHRC), McLean, VA (the sand bed surface mapping data after each bridge scour test was taken and provided by Mr. Oscar Suaznabar, Research Engineer from TFHRC, GENEX Systems). All the tests were completed during June 4-8, 2012. Specifically, the minimum flow velocities to set smart rocks of various size and density in motion were first characterized in the small flume. Natural rocks with one embedded magnet each (passive smart rocks) and acrylic balls with embedded electric circuits and electronics, batteries, and receiving/transmitting antennas (active smart rocks) were then characterized in the small flume for localization of the rocks as they slide or rotate mainly in one direction. Finally, smart rocks were validated for maximum scour depth monitoring in the large flume with two small-scale bridge pier models.

When placed on a hard flat floor with glued-on sand particles, acrylic balls with one embedded magnet each were found to set in motion at various water flow velocities, depending on their size and density (a 6.35 mm × 12.7 mm Grade N42 magnet embedded in a 15.9 mm-dia ball versus a 11.1 mm × 25.4 mm Grade N42 magnet in a 28.6 mm-dia ball). For example, the 28.6 mm-dia ball started to move at a flow velocity of 56 – 65 cm/sec. Based on the estimated velocity of 50 cm/sec around the rectangular bridge pier model to be tested for scour monitoring, the 28.6 mm-dia ball was considered as an appropriate design of passive smart rocks. This design was verified in the large flume to ensure that the 28.6 mm-dia ball does not move on a soft sand bed at approximately 50 cm/sec but moves and rotates while being scoured. Due to the size and density requirements of electronic components and batteries for underwater tests, active smart rocks were built with a PCB board with electric circuits and electronics, receiving/transmitting antennas, batteries, and coated brass balls embedded in a hollow acrylic ball of 63.5 mm in diameter. To save battery power, the electrical and electronic system remained off unless it was ready for test; it was turned on by a “magnet” switcher.

One or two passive smart rocks that move horizontally along with the water flow in the small flume can be detected individually in terms of sliding and rotation. When five passive smart rocks were deployed around the rectangular model bridge pier, it became a challenge to trace their individual movement. All passive sensors designed with magnets embedded inside the acrylic balls automatically rolled into the bottom of a scour hole and aligned themselves in contact as scour developed gradually. The deployment of multiple rocks can thus increase the magnetic field strength, which may allow the measurement at a large distance in applications. These tests validated the concept of passive smart rocks for scour monitoring.

Two active smart rocks were tested in the laboratory and demonstrated for the following functions: a) waterproof / sinking properties, b) communication using assigned IDs, c) wake up / data acquisition by timer, d) low power consumption (no battery issues occurred), e) effective antennas tuning, and f) localization / calibration accuracy. The proposed localization / calibration algorithm and procedure can locate a smart rock within 15 cm. Individual smart rocks in a group can be identified and detected with the designed and fabricated antenna and data acquisition system.

I - TECHNICAL STATUS

I.1 ACCOMPLISHMENTS BY MILESTONE

Task 1.1 Optimal Passive Smart Rock – Engineering Design and Validation of DC Magnetic Passive Smart Rocks

Specific Objectives

In the past quarter, prototype smart rocks were built and prepared for their characterization and validation tests in the Hydraulics Engineering Laboratory at Turner-Fairbank Highway Research Center (TFHRC), McLean, VA. First, the minimum flow velocities to set smart rocks of various size and density in motion were characterized in a small flume. Second, natural rocks with one embedded magnet each were then characterized in the small flume for localization of the rocks as they slide or rotate mainly in one direction. Finally, smart rocks were validated for maximum scour depth monitoring in a large flume with two small-scale bridge pier models. Following is a brief summary of the laboratory test results and preliminary analysis.

Minimum Water Flow Velocity to Set Smart Rocks in Motion: Three magnets of various sizes were embedded into acrylic balls to function like passive smart rocks. Each ball was individually tested in the small flume at the TFHRC as the velocity of water flow increased. The minimum velocity to set the ball in motion was recorded. It was concluded that the 11.1 mm × 25.4 mm Grade N42 magnet embedded in a 28.6 mm acrylic ball can resist the dragging force of water flow at 56 - 65 cm/sec when placed on top of the sand particles glued to a flat bottom of the small flume, which is slightly above the velocity (~50 cm/sec) around the small-scale bridge piers to be tested in the large flume. In practical design, the minimum water flow velocity depends on the size and density of smart rocks as well as the water flow condition in the river.

(a) Bottom texture of the flume (upstream) (b) Acrylic ball with an embedded magnet

Fig. 1 Minimum velocity test of various passive smart rocks

Localization Tests in Small Flume: To locate a smart rock, the magnetic field strength-distance curves for several controlled modes of the rock movement were recorded and used as basic patterns of the strength-distance curve for any general rock movement. Therefore, a magnet was

oriented either vertically or horizontally and tested as it moved away from a magnetometer in an open field at Rolla, MO. Figs. 2(a, b) illustrate the test setup and magnet movement. Figs. 3(a, b) show the change in magnetic field strength starting from approximately 38 cm away from the magnetometer through 60 cm. This range covered the measurement distances used during the small-scale scour monitoring tests in the large flume at TFHRC.

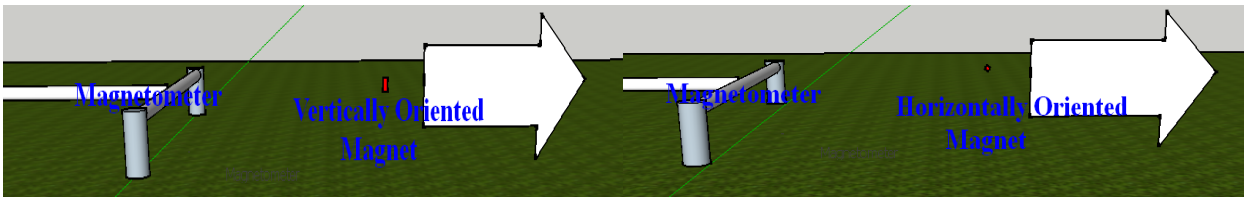

(a) Vertical orientation of magnetometer sensors (b) Horizontal orientation of the sensors

Fig. 2 Strength-distance correlation test layout

It can be seen from Fig. 3 that the shapes of the two overall curves (shown in inserts) are similar. However, the vertical orientation gives more sensitive measurements than the horizontal orientation. For example, in the distance range of interest to the small-scale bridge pier tests, the magnetic field strength dropped 1100 nT over 23 cm in the vertical orientation and 900 nT over 25 cm in the horizontal orientation. Also note that there is an ascending stage of the strength when the magnet was oriented horizontally.

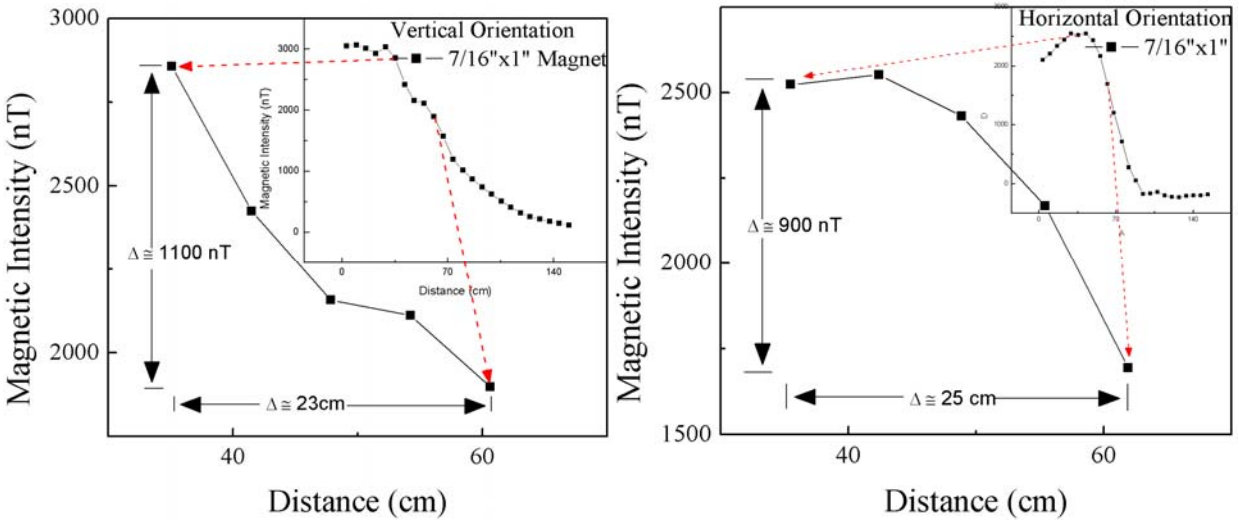

(a) Vertical orientation data (b) Horizontal orientation data

Fig. 3 Strength-distance curves

Small Flume and Passive Smart Rock: The small flume used for various characterization tests of passive and active smart rocks is shown in Fig. 4(a). The velocity of water flow in the flume can be adjusted by simultaneously regulating the power of two hydraulic pumps and the angle of tail plates (see insert) at both ends of the flume. For characterization tests, passive smart rocks were made by drilling an oversize hole on a natural rock, placing a magnet into the natural rock and sealing the hole with a Great Stuff TM by DOW sealant as shown in Fig. 4(b). The magnet was embedded into the rock to demonstrate the flexibility of passive sensor encasement options and the reliability of passive sensors within the natural rock structure.

(a) Small flume at TFHRC (b) Natural rocks with and without an embedded magnet

Fig. 4 Overview of the small flume and a passive smart rock

Three test cases with one, two, or three smart rocks were considered in the flume with controllable water flow velocities. For each case, the flow velocity was increased until the passive smart rocks moved. For example, Fig. 5 displays the movement of two smart rocks as the velocity increased. The magnetometer was placed nearby as shown in Fig. 6 and took a continuous reading for each of these tests at 0° (the line of two sensors is perpendicular to the water flow direction).

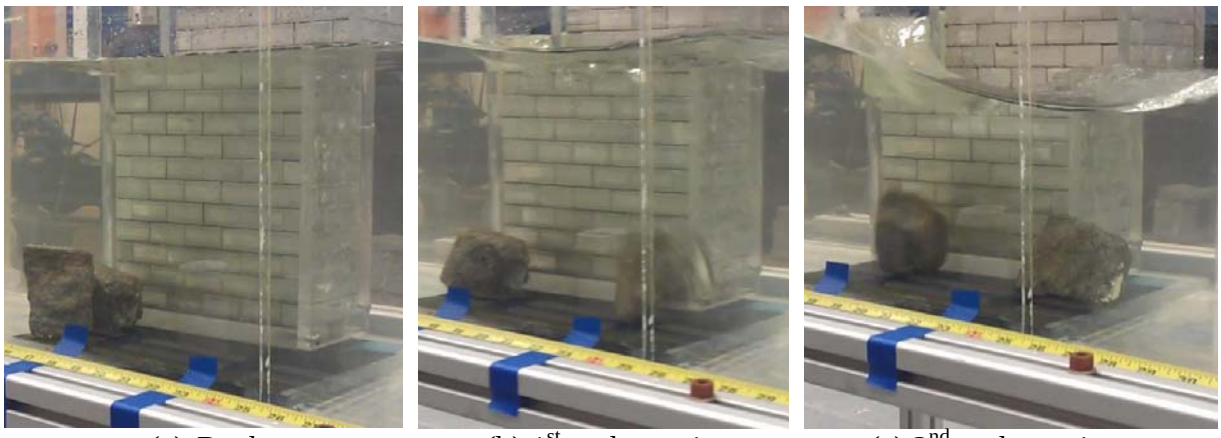

(a) Rocks at rest (b) 1st rock rotating (c) 2nd rock moving

Fig. 5 Movement of two rocks at various flow velocities

(a) Small flume tests (b) Small-scale bridge pier tests in large flume

Fig. 6 Measurement with a magnetometer

The effects of rock distance, orientation, and group on magnetic field strengths were quantified in the small flume at TFHRC. To simulate a turbulence flow, an artificial block was placed inside the flume to locally increase the flow velocity as illustrated in Fig. 5.

One Smart Rock: Fig. 7(a) shows the magnetic gradient measurement from one smart rock (one magnet). Before 00:08, the smart rock was rocking back and forth at low amplitude, causing a low level disturbance on the magnetic field measurement. It was then sliding over some distance and finally rotated before it was slowly sliding away from the magnetometer.

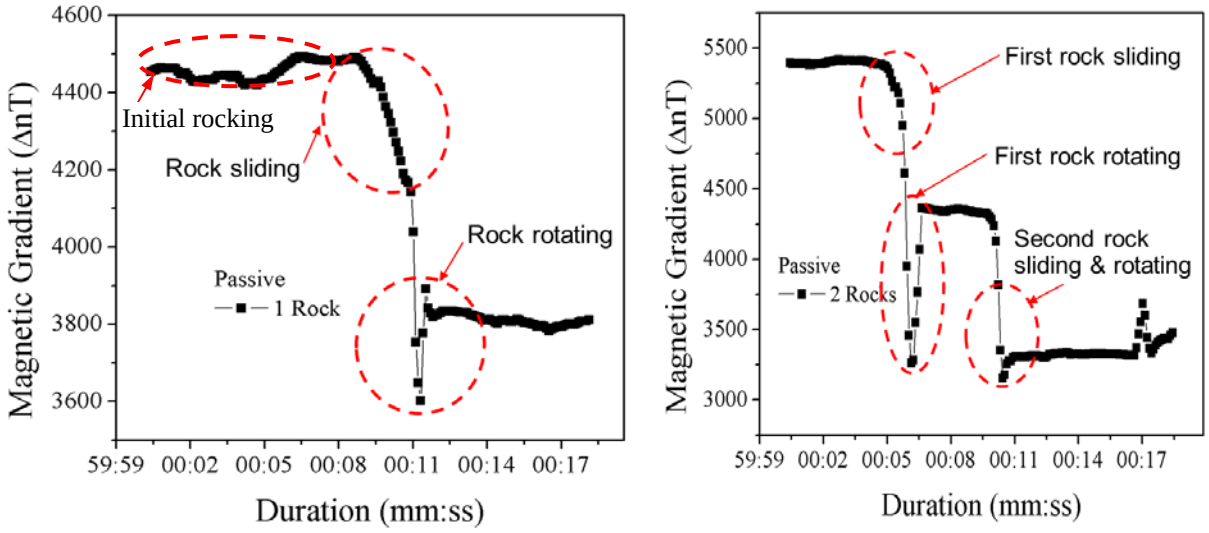

(a) One passive rock b) Two passive rocks

Fig. 7 Test results: magnetic field gradient vs. time

Two Smart Rocks: The magnetic gradient measurements from the two smart rocks are presented in Fig. 7(b). As one can see, the first rock did not slide until around 00:05. Immediately after the initial sliding, the rock rotated under the increasing water flow. The first rock then remained at the same location. Meanwhile, the second rock began to slide at approximately 00:09. Immediately after that moment, the second rock almost rotated under the strong flow and then remained at the same position.

Small-Scale Bridge Scour Tests: Two small-scale bridge piers, circular and rectangular, were tested in a large flume as shown in Fig. 8 to validate the proposed smart rock technology in the laboratory condition. The magnetometer was placed on a platform above the bridge piers to simulate testing from the bridge deck. In order to determine if the change in magnetic field strength was due to rock moving or rotating, multiple measurements were taken approximately every 30^{o} for each reading period. A reading was recorded every ten minutes for the duration of the test which lasted approximately one and a half hours.

Throughout the scour test, visual observations on the development of the scour hole were made continuously for about 30 minutes and periodically afterward. It was visually observed that the scour depth continuingly increased for a period of 1.5 hours. About 70% of the scour hole was developed in the first half an hour. Smart rocks placed around the piers rolled at different times and then remained at the bottom of the scour hole developed over time.

Fig. 8 Overview of the test setup and details of magnet placement and measurement

One Smart Rock: One acrylic ball with an embedded magnet was placed in front of the rectangular pier as illustrated in Fig. 9(a). The model pier is 225 mm long (water flow direction), 750 mm wide, and approximately 500 mm.

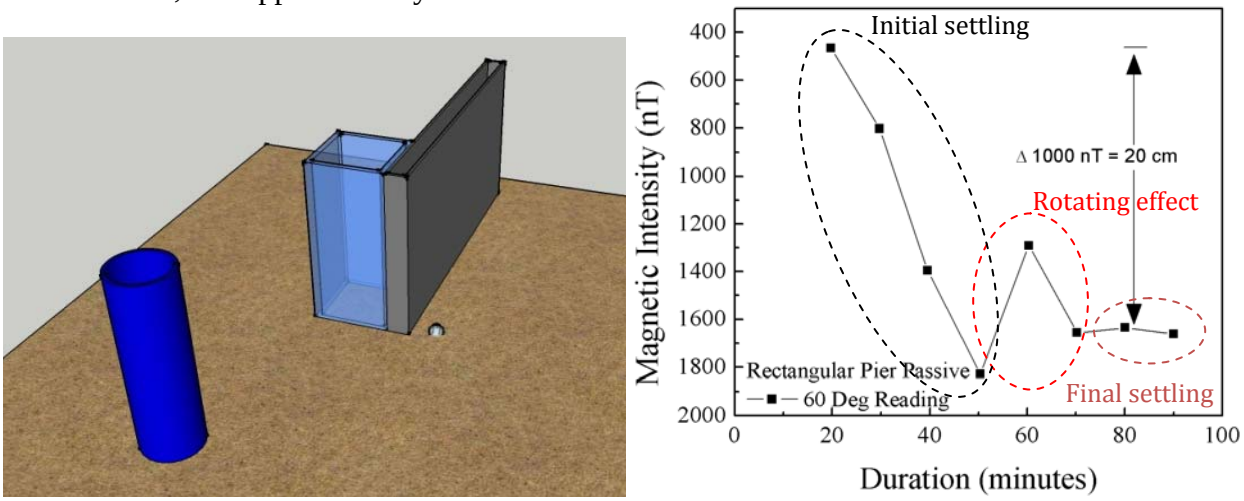

(a) Location of one smart rock (b) Strength change over time with strength-distance correlation

Fig. 9 Test setup and results with the first scour test

Fig. 9(b) shows the change in magnetic field strength over time when the upstream flow velocity was 27 cm/sec. The overall change is approximately 1000 nT, which corresponds to a distance change of approximately 20 cm when compared with the previous test data in Fig. 3. The post-test surface map taken from a laser device at 20 cm above the riverbed and the deepest points profile of the sand bed (D_{50}=1 mm), Figs. 10 (a – c), confirm that the maximum scour at the rectangular pier was approximately 18 cm. The maximum scour depth was also verified by the post-test measurements as given in Fig. 11. Note that the blue line and green line in Fig. 10(a) represent the x–axis and y–axis deepest scour locations, respectively.

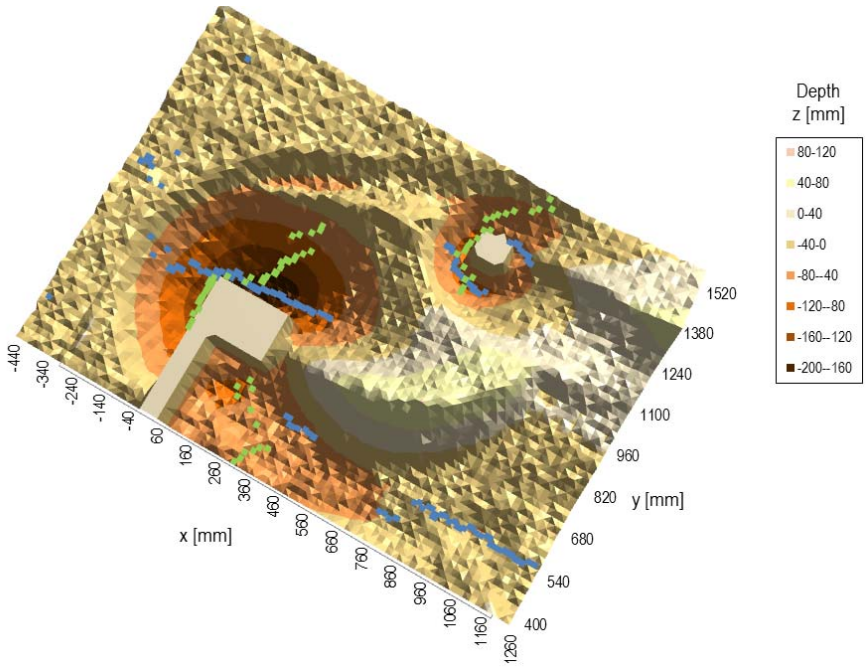

(a) Surface mapping of the sand bed after the scour test

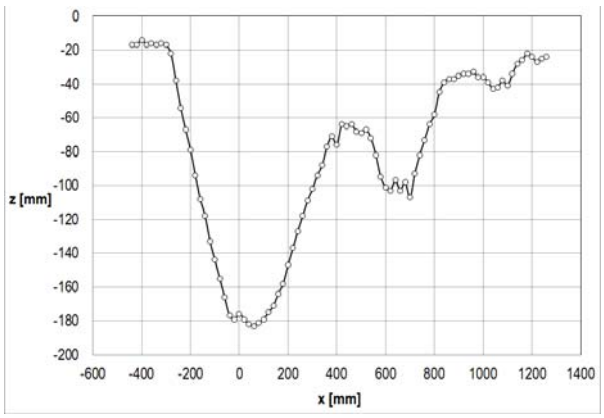

(b) x–axis deepest point profile

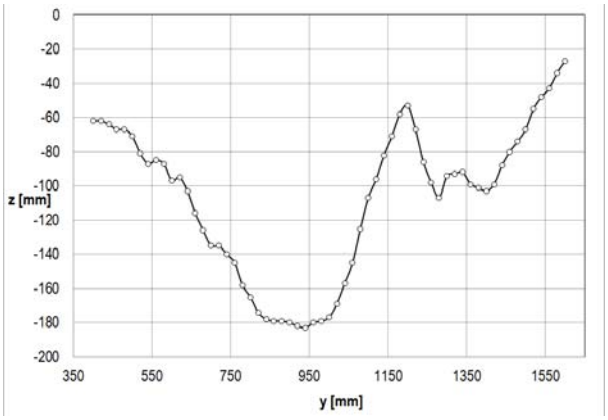

(c) y–axis deepest point profile

Fig. 10 Post-test surface mapping results for test one

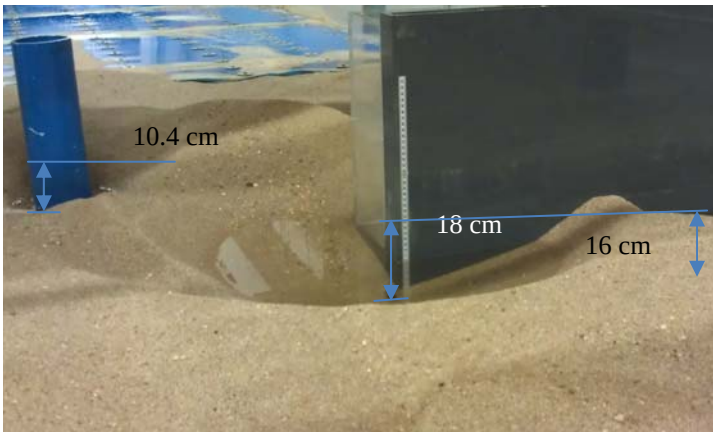

Fig. 11 Maximum scour depth at the completion of the test

Two Smart Rocks: One acrylic ball was placed in front of the rectangular pier and the other ball in front of the circular pier as shown in Fig. 12(a). The circular pier was 114.3 mm in diameter, and located 490 mm and 480 mm from the rectangular pier and the glass wall, respectively. It was situated downstream of the front face of the rectangular pier by 297 mm.

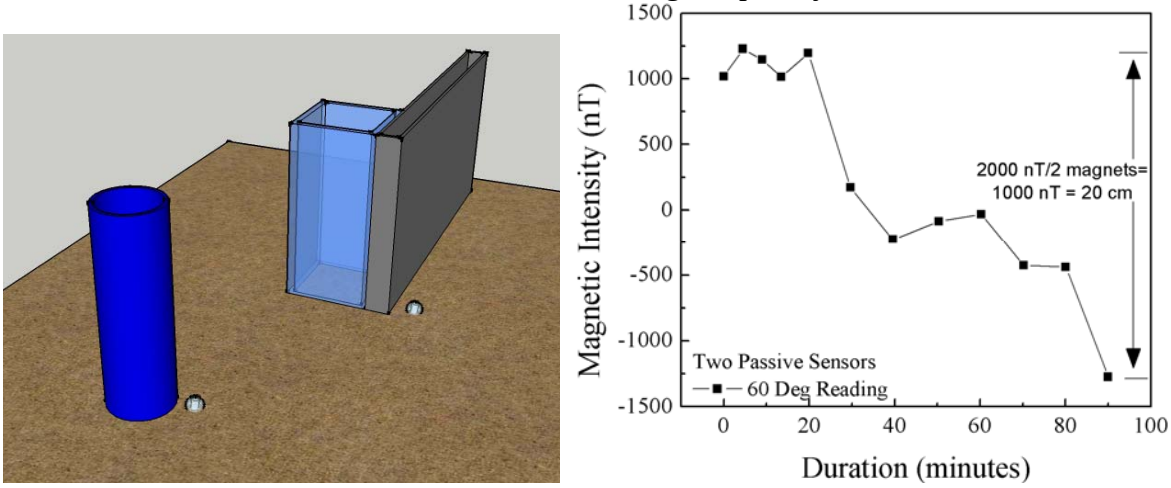

(a) Location of two smart rocks (b) Strength change over time with strength-distance correlation

Fig. 12 Test setup and results from the second scour test

Fig. 12(b) shows the change in magnetic field strength over time when the upstream flow velocity was 27 cm/sec. The overall change by the two rocks is 2000 nT, each contributing approximately 1000 nT. Like the first scour test, this result corresponds to a distance change of approximately 20 cm. The post-test surface map and the deepest points profile of the sand bed, Figs. 13 (a – c), also confirm that the maximum scour at the rectangular pier was approximately 18 cm. However, the maximum scour depth at the circular pier is only approximately 11 cm. The magnetometer cannot distinguish between two different readings and the strength represents the combined effect of all magnetic interferences within the area. This makes it difficult to determine the depth of an individual passive smart rock if placed at different piers. This will not pose a problem in practice as bridge monitoring can be planned for one pier or two well-separated piers.

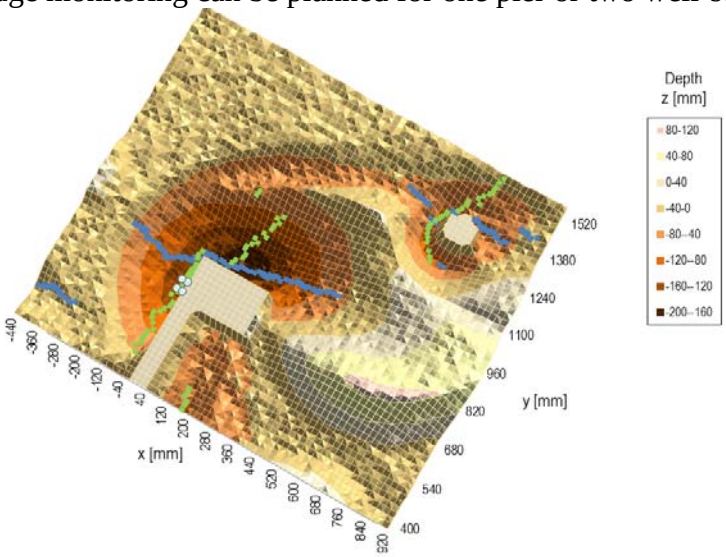

(a) Surface mapping after the scour test

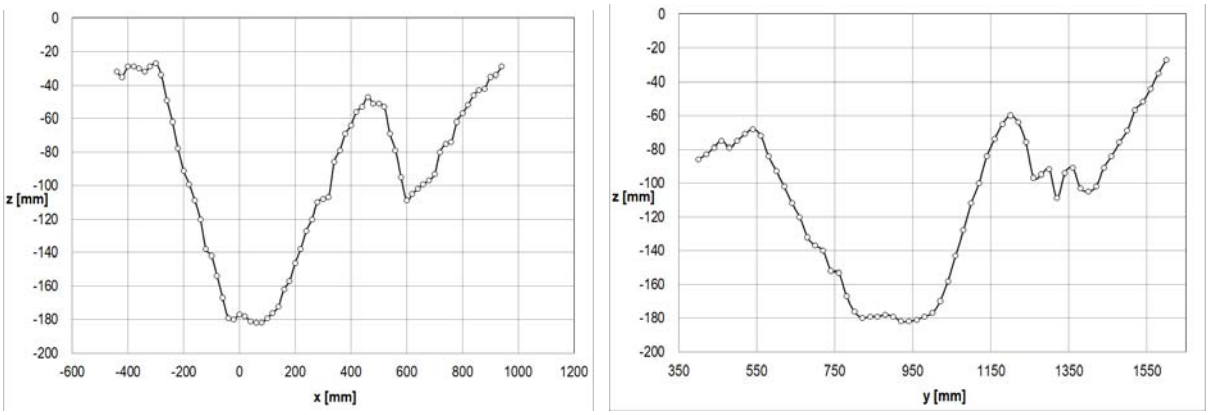

(b) X - axis deepest point profile c) Y – axis deepest point profile

Fig. 13 Post-test surface mapping results for test two

Five Smart Rocks: The final test setup consisted of five passive smart rocks around the rectangular bridge pier in various locations and one active sensor at the circular bridge pier. Fig. 14(a) focuses on the passive sensors around the rectangular pier. Readings were taken after each passive sensor moved and joined another or every ten minutes until the final passive sensor, placed 28 cm away from the bridge pier, rolled into the scour hole and connected with the other passive sensors. Four sensors were placed directly in front of the rectangular bridge pier and connected together within the first 30 minutes of the test.

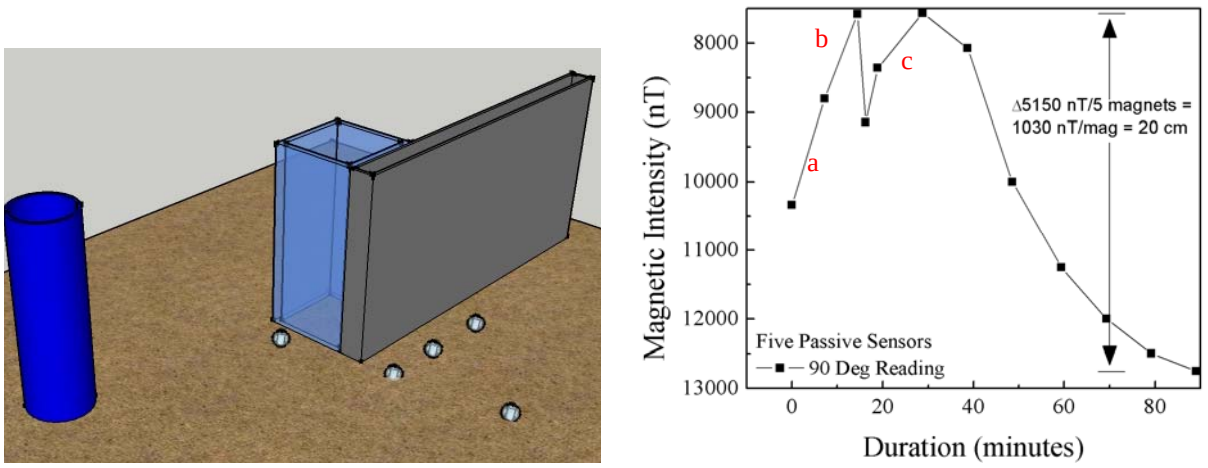

(a) Location of five smart rocks (b) Strength change over time with strength-distance correlation

Fig. 14 Test setup and results from the third scour test

Typically, the magnetic field strength doesn't increase drastically as a passive rock moves away from the magnetometer. In this case, however, as the passive rocks attached to each other, the magnetic strength actually increased. The red letters (a–c) in Fig. 14(b) correlate with the scour models in Fig. 15(a–c). Fig. 15 also illustrates the ability of the passive smart rocks to find the maximum scour location. The back smart rock actually rolled against the current to the bottom of the scour hole. The final location and orientation of the smart rocks can be seen in Fig. 15(d).

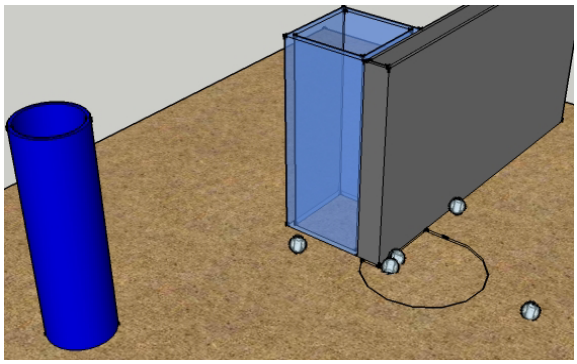

(a) First two sensors connect

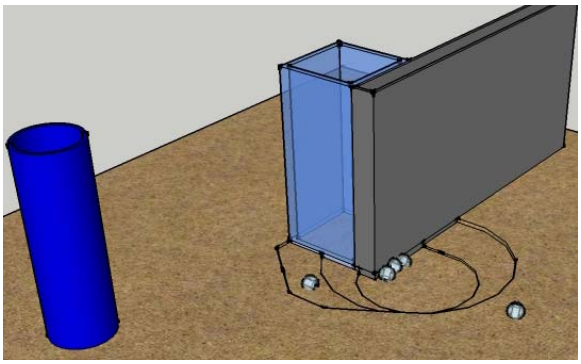

(b) Third sensor connects to the first two

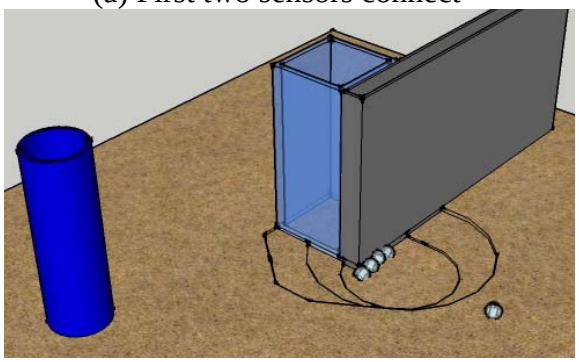

(c) Fourth sensor rolls against the current and attaches to the three connected sensors

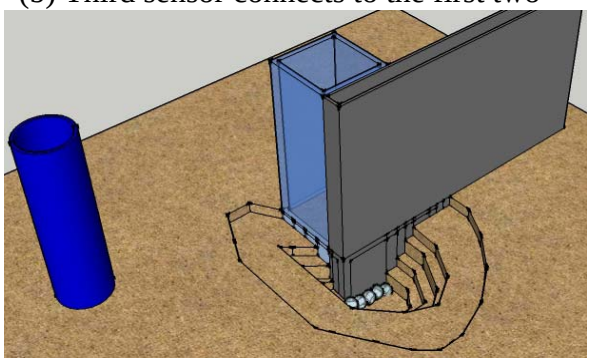

(d) Fifth sensor rolls to the bottom of the scour hole to attach to the other sensor

Fig. 15 Characteristic behavior of passive smart rocks in a scour event

Since there are five passive smart rocks within range of the magnetometer, the change in magnetic strength should be approximately five times greater than the correlated distance graph of Fig. 3. Fig. 14(b) shows a result of approximately 20 cm maximum scour depth, which is confirmed by the surface mapping results of Fig. 16.

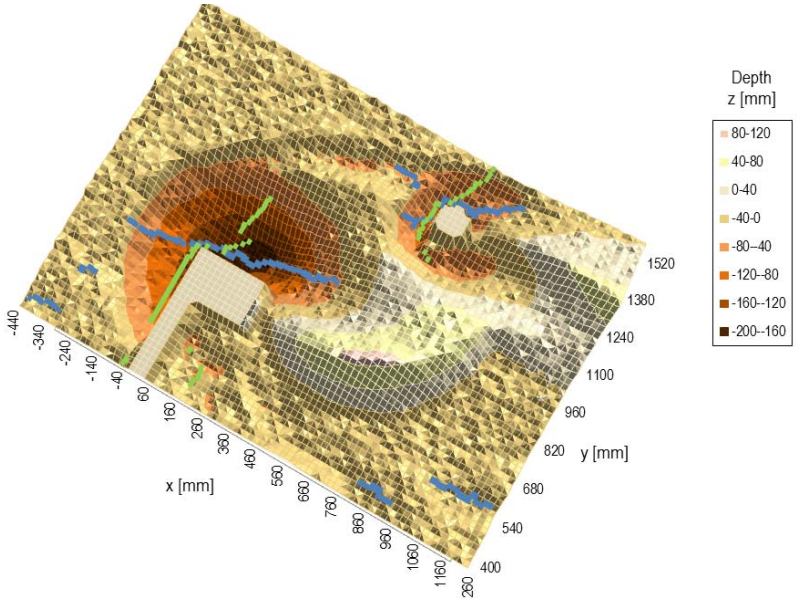

(a) Surface mapping after the third scour test

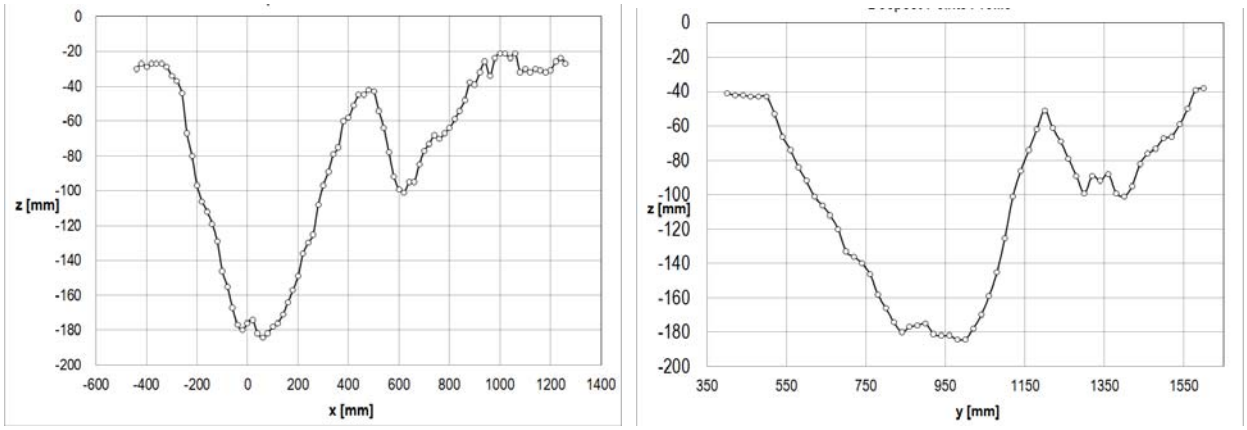

(b) X–axis deepest point profile (c) Y–axis deepest point profile

Fig. 16 Post-test surface mapping for test three

Preliminary Conclusions with Passive Smart Rocks: All three scour simulations result in the same scour depth correlation. This repeatability is very promising for the validity of the passive smart rocks. During the scour tests, the designed smart rocks always rolled and remained at the bottom of a scour hole, giving the maximum scour depth. One to three smart rocks placed near a bridge pier can potentially be located individually by multiple measurements at various angles. However, five smart rocks are difficult, if not impossible, to distinguish from magnetic field strength measurements.

Task 1.2 Steel Interferences to Magnetic Measurements – Noise Level, Data Cleansing and Engineering Interpretation with Passive Rocks Submitted

Fig. 17(a) compares the individual readings from the two sensors of a magnetometer. Their difference was presented in Fig. 7(b) as magnetic gradient. For a convenient comparison, the reading from the closest sensor was reproduced in Fig. 17(b). By comparing Fig. 17(b) with Fig. 7(b), it is observed that the gradient mainly removed the Earth's magnetic field. There is no clear sign of indication that the noise level in the gradient readings was reduced by the subtraction.

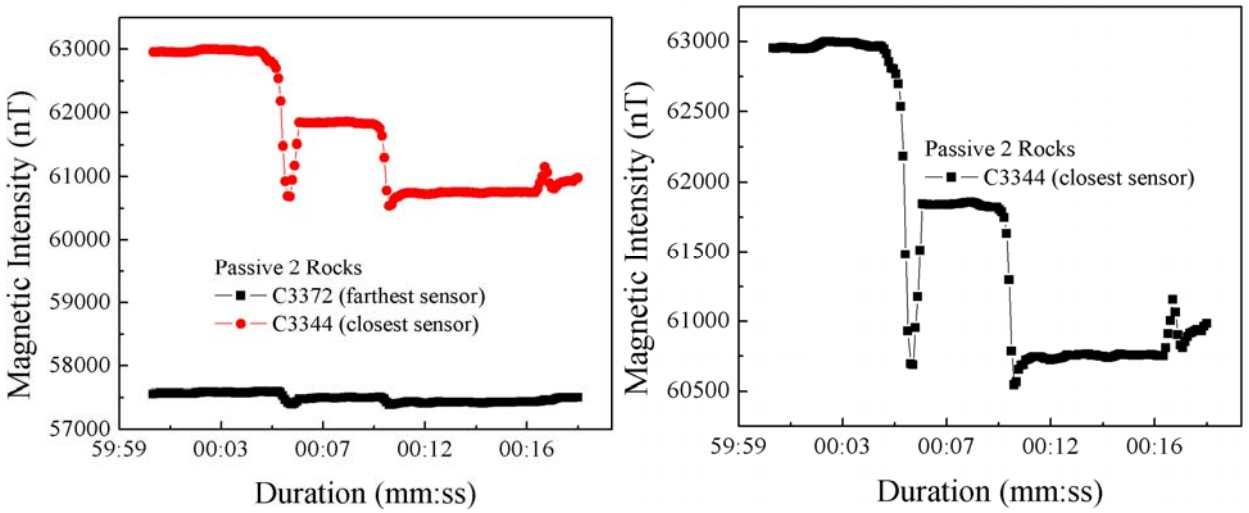

Fig. 17 Comparison between individual and gradient readings

Task 2.1 Active Smart Rocks with Embedded Controllable Magnets or with Embedded Electronics – Engineering Design and Validation of Active Smart Rocks Submitted

There is no report on this task during the past quarter.

Task 2.2(a) Magneto-Inductive Communications – Engineering Design and Validation of Magneto-Inductive Transponders Submitted

Smart Rock 2.4 Assembly A smart rock board was enclosed into a hollow acrylic ball of 2.5" in diameter as shown in Fig. 18. It included the version 2.4 electronic modules: a PCB with electronics circuit, receiving/transmitting coil antenna, two CR123A batteries in parallel, and many solid brass balls (~3.5 mm diameter) required to ensure that the assembled unit (> 160 grams) remains at the bottom of the flume during tests. The brass balls were first painted with a non-conductive coating to avoid any electric conductive contact and then were glued inside the acrylic ball using a hot glue gun. The coil antennas integrated into the assembly were placed perpendicularly to the smart rock electronic board to reduce the chance for possible detuning of the antenna by metal parts of the board. The acrylic ball was sealed using silicone adhesives and tight wrapping with electric tapes for underwater applications.

Four smart rock units were used during the laboratory tests. Two of them were programmed for continuous acquisition and transmission with a predefined timer delay; the other two were programmed in response to external wake-up calls. Data transmission and processing were performed using analog signal processing procedures during tests. But transmission was made following the RS232 protocol in ASCII code without data encoding/compression and error recovery for future implementation with digital signal processing routines.

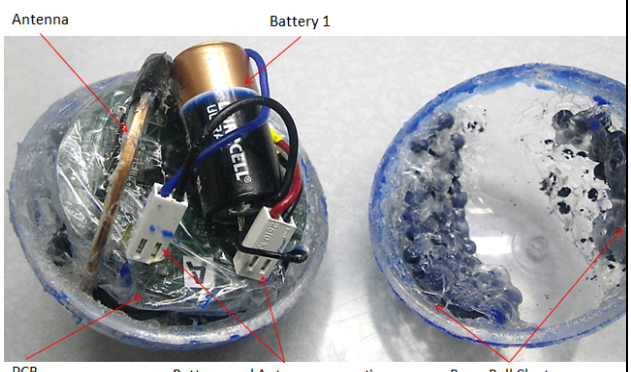

Fig. 18 Smart Rock 2.4 assembly

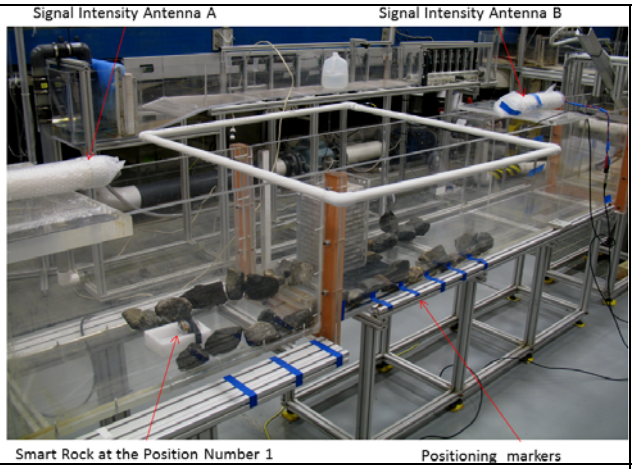

Fig. 19 Antennas and active smart rock

Test Setup Fig. 19 shows the setup of various tests in the small flume. The smart rock was placed at the bottom of the flume in between a group of natural rocks (the smart rock as shown in Fig. 19 was placed in the styrofoam box for calibration tests only). The natural rocks were used to create local turbulence and various patterns of the smart rock motion. Two antennas A and B were placed on top of the flume tank at the ends of the measurement areas to detect the receiver signal strength intensity (RSSI) for further localization since the smart rock generally moved

along the flume tank in one direction for this test. However, the base station control system as illustrated in Fig. 20 can support and process up to four antennas. For data acquisition of the smart rock (pitch, roll, heading), a large square loop antenna was placed in the middle area of the measurement area over the water flow. Thus, the control PC was connected to a data channel demodulator unit and to the oscilloscope, providing RSSI estimates from localization antennas.

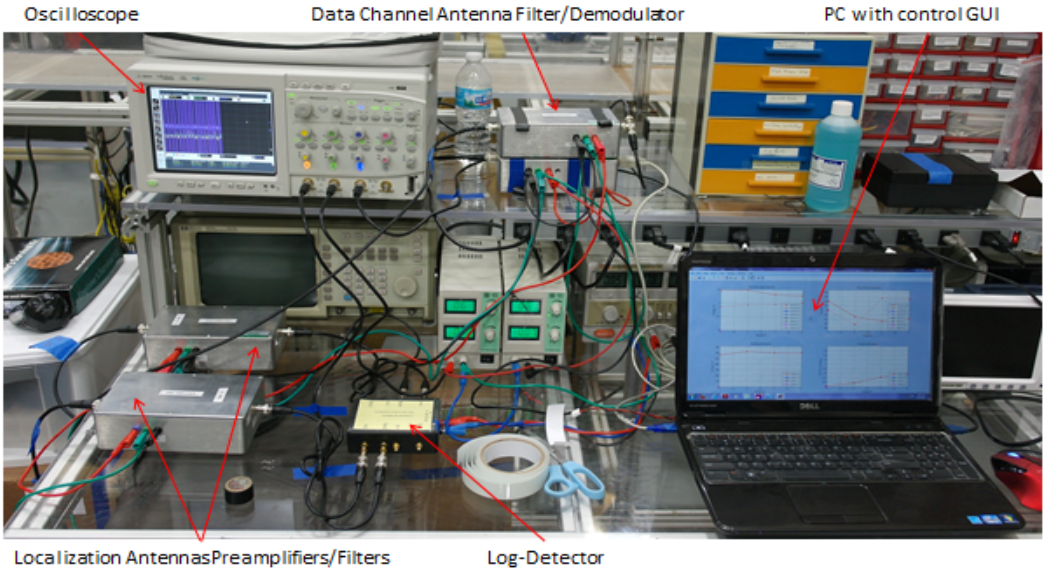

Fig. 20 Base station control area

In addition to the base station control area with analog signal processing units (preamplifiers, filters and demodulators), Fig. 20 also shows a log-detector, an oscilloscope and a PC with Control GUI in Matlab. The electronic units were powered by bench power supplies during the tests. However, they will be better integrated and packaged into a portable system in the future.

Calibration Tests To facilitate the localization of smart rocks, the RSSI trends from the test setup in Fig. 19 were calibrated in the laboratory environment with the predetermined locations of smart rocks. In general, the presence of external electronics, power supplies, chargers, high-speed cameras, pump controllers and motors makes the hydraulics laboratory a noisy environment from an electromagnetic point of view. In such a noisy environment, the signal-to-noise ratio of smart rocks is expected to degrade. During a calibration test, a sample smart rock was manually placed at one of the 16 predetermined positions with approximately 7 cm in spacing, as marked by blue tapes in Fig. 19. At each position, three perpendicular orientations of the smart rock were tested and the RSSI readings from the antennas A and B shown in Fig. 19 were saved. For convenience, X-orientation is designated along the water flow in the small flume, and Y-orientation and Z-orientation are perpendicular to X-orientation in horizontal and vertical directions, respectively. For each test condition, three repeated runs were conducted.

Fig. 21(a-c) show the average RSSI antenna reading for each orientation and Fig. 21(d) presents the overall average of the Antenna A to B RSSI ratios in all three orientations as a function of the rock position. It can be observed that the RSSI-position relationship was basically linear from position 3 to 16 and used as reference data for the localization of smart rocks that may be oriented in any direction in general cases.

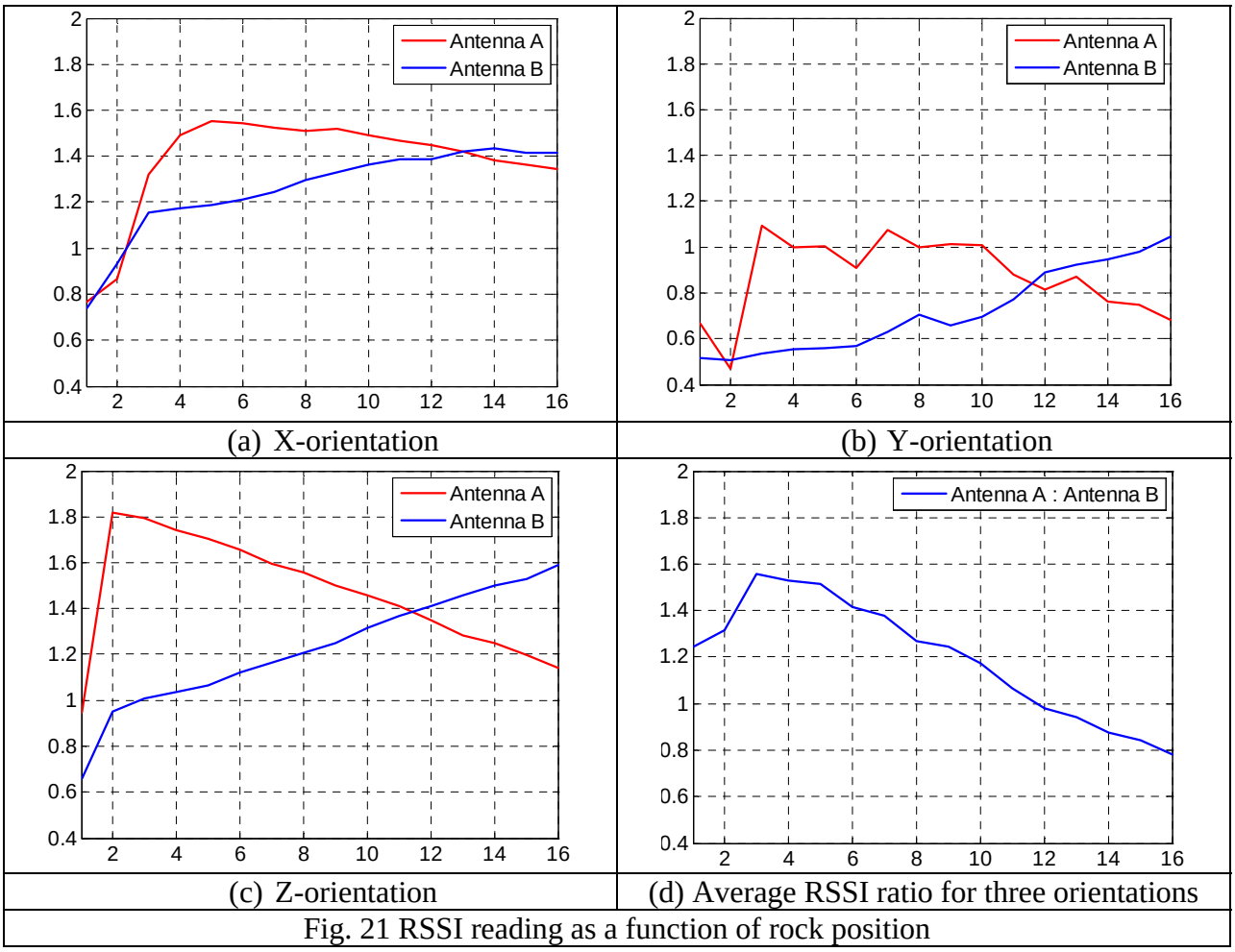

(a) X-orientation (b) Y-orientation

(c) Z-orientation (d) Average RSSI ratio for three orientations

Fig. 21 RSSI reading as a function of rock position

General Tests, Results, and Discussion To test the functionality of various sensors, two active smart rocks with external wake-up signal processing were moved manually one-by-one inside the small flume at 30-40 cm steps. In each position, data from every rock was collected from individual rocks. The last step was to return the two rocks to their start positions, respectively. Fig. 22 shows a screenshot from the Control GUI with the RSSI data, pitch, roll, heading and the estimated position information from the RSSI readings and the calibration curves. Sample #1 and #6 represent the start and end positions of the two rocks, respectively. The top left graph displays the RSSI readings from Antenna 1 (A in Fig. 19) in solid curve and from Antenna 2 (B in Fig. 19) in dashed line. The top right graph shows pitch in solid curve and roll in dashed line for smart rocks. Note that the control interface supports a simultaneous visualization of the data from four smart rocks (A to D) and only A and B were used in this test.

It can be seen from Fig. 22 that there was no sign of significant change in pitch, roll and heading since the two rocks were moved manually. The position information from each rock shown in the bottom right graph was in good agreement with the physical locations of the rocks during tests. In particular, the accuracy of position estimation seems to be ±15 cm as indicated in the comparison between samples #1 and #6.

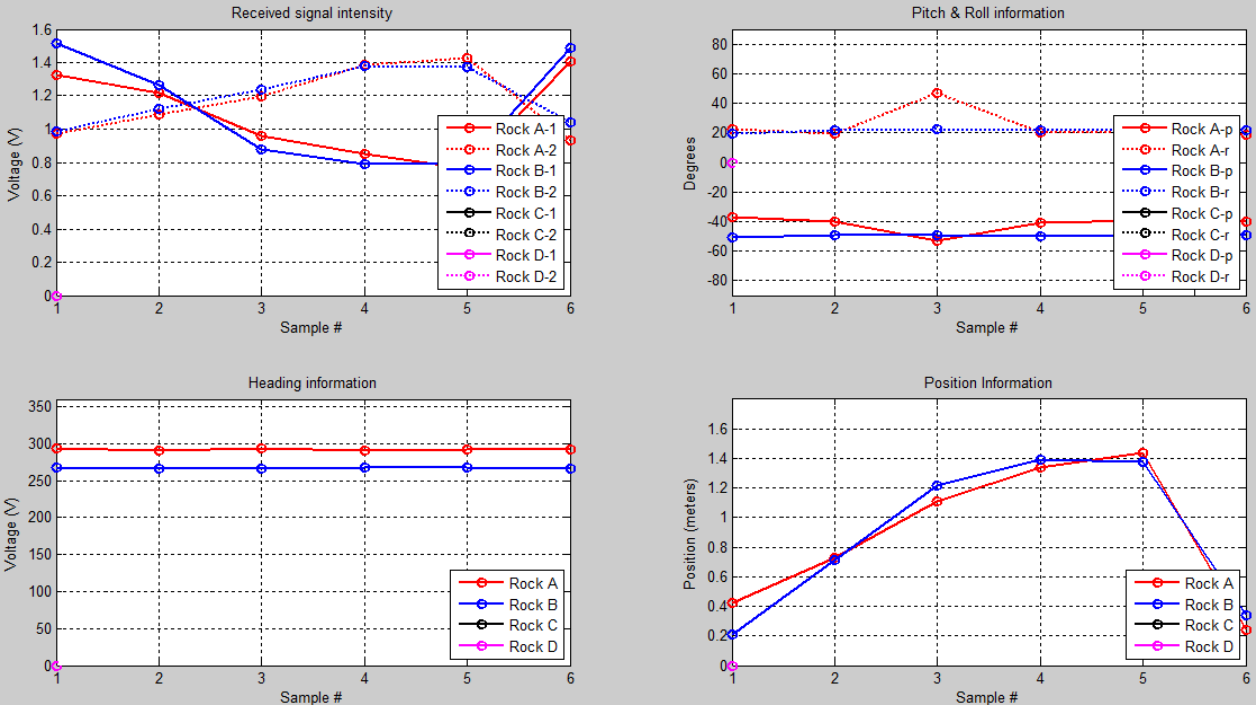

Fig. 22 Data from two active smart rocks moved manually in the small flume

General tests were performed by placing two smart rocks in the small flume and letting them move along with the water flow between the Antennas A and B shown in Fig. 19. The time required to complete one test varied from 10 second to several minutes, depending on the water flow velocity. As shown in Fig. 19, natural rocks were also placed in the flume to potentially create spatially-varying velocities and accelerate/decelerate the active smart rocks.

Fig. 23 shows the test results when one smart rock moved along the water flow. While the smart rock generally moved in the forward direction, the position information indicates possible moves of the rock opposite to the water flow. These local changes were likely attributed to the rocking motion (sample # 4-6) and lateral movement (sample # 6 to 7) of the smart rock, both causing an alternation of the RSSI readings from Antennas A and B. Sample #7 to 8 indicated that the rock was temporarily stuck at one position.

Fig. 24 shows the test results when two smart rocks were placed in the small flume and moved along with the water flow. It was visually observed that Rock 'A' traveled through the measurement area more rapidly than Rock 'B'. But Rock 'A' was stuck at the exit of the test range after the 5th step. Rock 'B' temporarily stopped in the middle of the flume when Samples # 4-7 were recorded. These physical observations are the evidences why there are 5 reading steps for Rock 'A' and 11 steps for Rock 'B' over the same travel distance. Overall, this general test case indicated that the position monitoring task with active smart rocks was performed successfully and the rock localization algorithm is stable and reliable.

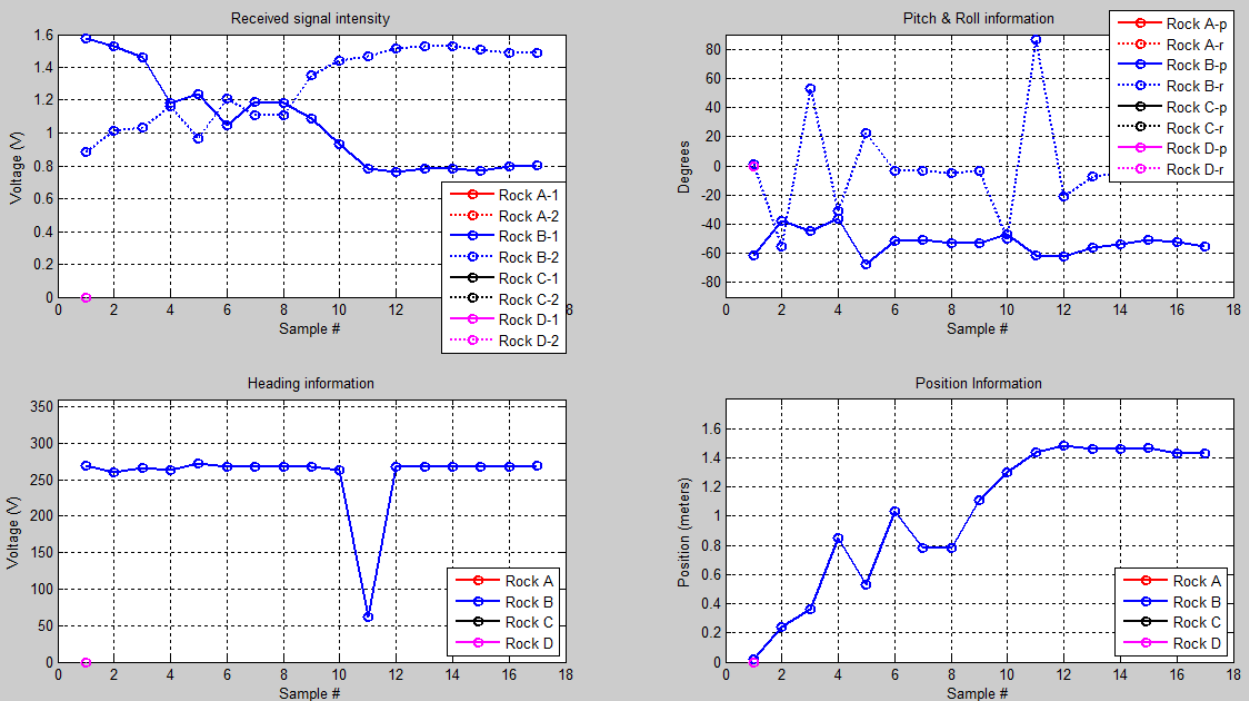

Fig. 23 Data from one active smart rock moved along the water flow

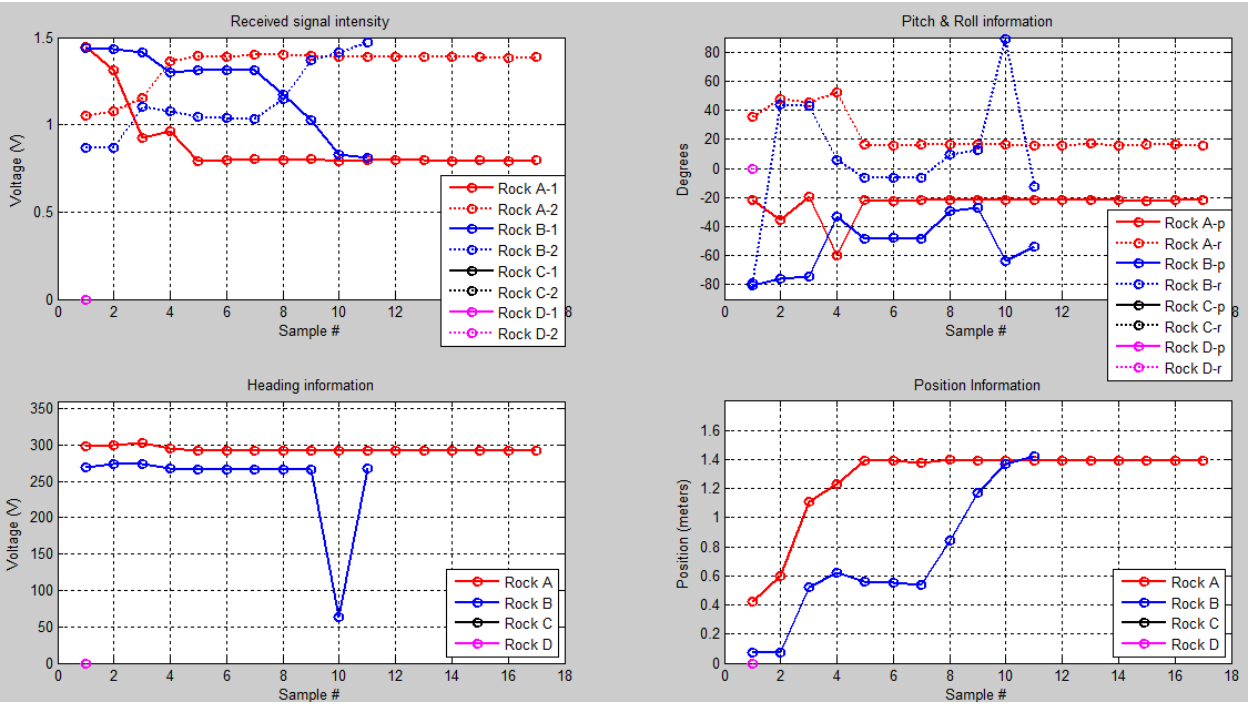

Fig. 24 Data from two active smart rocks moved along the water flow

Task 2.2(b) Acoustic Communications – Engineering Evaluation of Acoustic Communication Systems for Bridge Scour Monitoring

In this quarter, no report is included due to page limits.

Task 3.2 Field Validation Planning and Execution – Field Test Plan and Data Analysis Submitted

The research team met with the Missouri Department of Transportation and together they have identified four bridges for potential field tests over the performance period of this project. Two of the four bridges will be finalized for potential tests in August or September, 2012.

I.2 PROBLEMS ENCOUNTERED

During the laboratory tests on June 4-8, 2012, in the hydraulics engineering laboratory at TFHRC, it was found that one sensor of the magnetometer was malfunctional likely due to loose cabling. The manufacturer is currently being contacted for emergency repair of the equipment. Because of this, field tests expect to be delayed for about one month. The field test schedule will be finalized after the magnetometer has been received from the emergency repair.

In addition, one key student member in electrical engineering took an internship with a company in California, which is part of the important educational training for students. The post doctor position was recently filled. Overall, it is estimated that the project expects to be delayed for less than three months. On the other hand, the project expenditure is generally consistent with the project progress.

I.3 FUTURE PLANS

Three subtasks will be executed during the next quarter. A brief description of various activities in each subtask is described below:

Task 1.1 Design, fabricate, and test in laboratory and field conditions DC magnetic sensors with embedded magnets aligned with the earth gravity field. Summarize and document the test results and the performance of passive smart sensors.

Based on the laboratory tests on passive smart rocks with embedded permanent magnets, passive sensors with larger magnets will be built for bridge tests. Small sensors will also be built and tested for the automatic alignment function to enhance the smart rock sensitivity. Their effectiveness in providing sensitive magnetic field measurements will be systematically characterized.

Task 1.2 Research, summarize, and document the degree of potential steel interferences to magnetic measurements. Investigate ways to compensate the interference effect and develop a rock localization technique.

Further tests will be conducted in laboratory to see if noise effects are indeed significant with magnetic field measurement.

Task 2.1 Design, fabricate, and test in laboratory and field conditions active smart rocks with embedded controllable magnets or with embedded electronics. Summarize and document the test results and the performance of active smart rocks.

The design of active smart rocks with controllable magnets is being finalized. The test results will be reported during the following quarterly report.

Task 2.2(a) Design, fabricate, and test in laboratory and field conditions magneto-inductive transponders. Summarize and document the test results and the performance of transponders.

Currently the next version of smart rock electronic board is in design stage. Following updates are planned for further development works:

- PIC microcontroller upgrading. The new IC, PIC16LF1829, will provide 6 more Input / Output pins compared to the IC used in Smart Rock 2.4 and supply 8 times more memory for program firmware.
- 4 MB memory integration into the smart rock so that continuous readings can be first stored in memory and then transmitted together with other data (better log of events, faster processing, less power)
- Shake/move interrupt handling (wake up due to movement)
- Tunable capacitor integration for fine tuning of on-board receiving/transmitting antenna
- Inter-rock data exchange / smart rock network organization
- Schematic errors debugging and further software optimization
- Digital signal processing integration

Task 2.2(b) Research, summarize, and document current underwater acoustic transmission practices and required modifications for bridge scour monitoring.

In the following quarter, the acoustic communication system with transmitter and receiver will be refined. A multi-receiver system will then be built and tested with capability of smart rock localization. In this case, multiple transducers / hydrophones are distributed to different locations for TDOA estimation. The smart rocks will be located using the TDOA fusion and the assistance of pressure sensor in smart rocks, which provides the elevation information of the smart rocks. They will be ready for field testing of one or two bridges.

Task 3.2 Plan and execute the field validation tasks of various prototypes. Analyze the field performance of smart rocks and communication systems.

As prototype smart rocks are being built, field test plan will be developed in the following months.

II – BUSINESS STATUS

II.1 HOURS/EFFORT EXPENDED

The planned hours and the actual hours spent on this project are given and compared in Table 1. In the fourth quarter, the actual hours are approximately 22% of the planned hours due to student internship and short of staff appointed on this particular project. That is, the actual cumulative hours are approximately 36% of the planned hours. The cumulative hours spent on various tasks by personnel are presented in Fig. 25.

Table 1 Hours Spent on This Project

	Planned		Actual	
	Labor Hours	Cumulative	Labor Hours	Cumulative
Quarter 1	752	752	184	184
Quarter 2	752	1504	345	529
Quarter 3	752	2256	381	909
Quarter 4	752	3009	166	1075

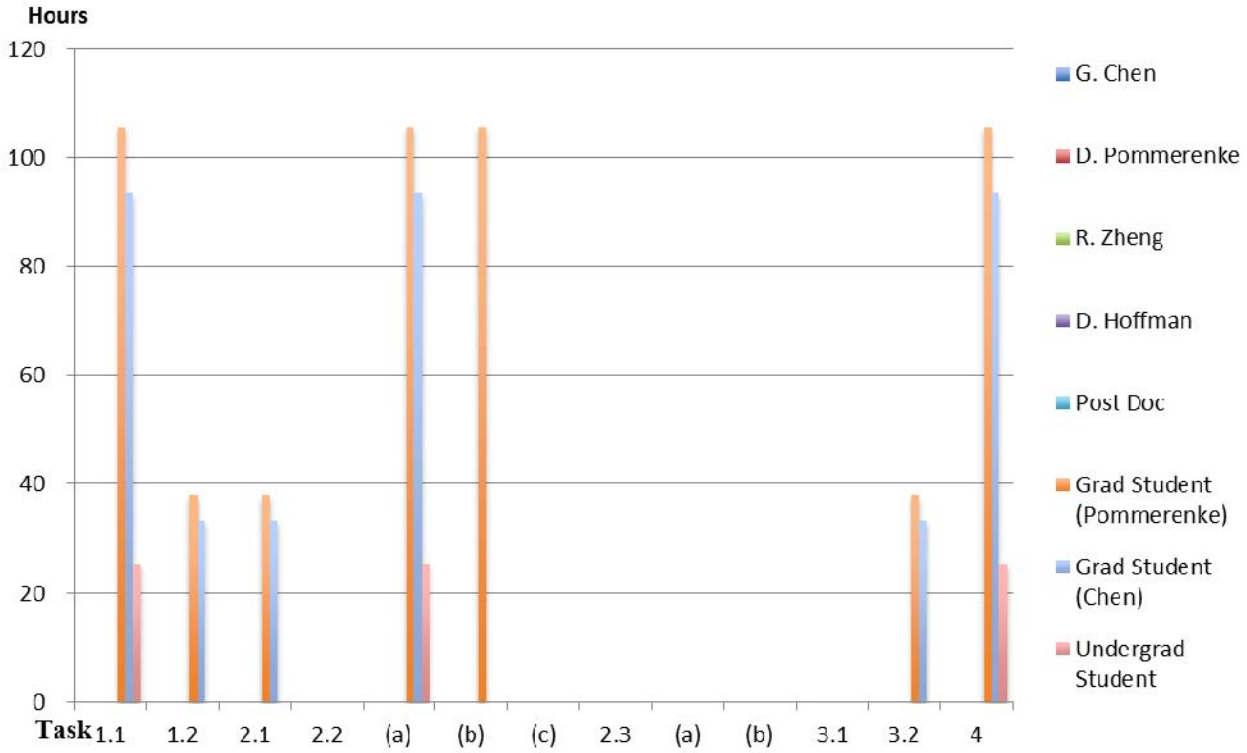

Fig. 25 Cummulative hours spent on various tasks by personnel

II.2 FUNDS EXPENDED AND COST SHARE

The budgeted and expended RITA funds in each quarter are compared in Fig. 26. Approximately 42% of the budget has been spent during the fourth quarter. The actual cumulative expenditures from RITA and Missouri S&T are compared in Fig. 27. The expenditure from RITA is approximately 100% of that from the Missouri S&T.

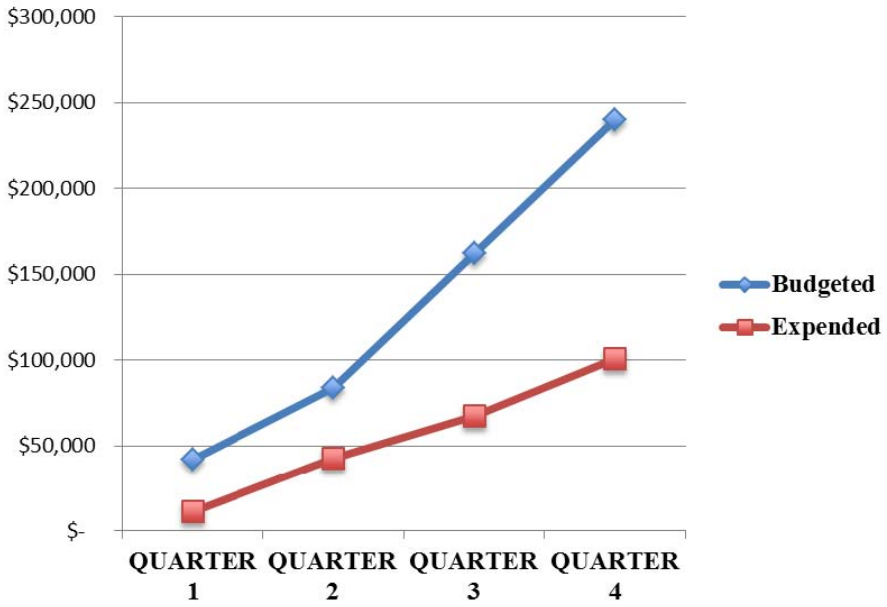

Fig. 26 RITA budget and expenditure comparison in every quarter

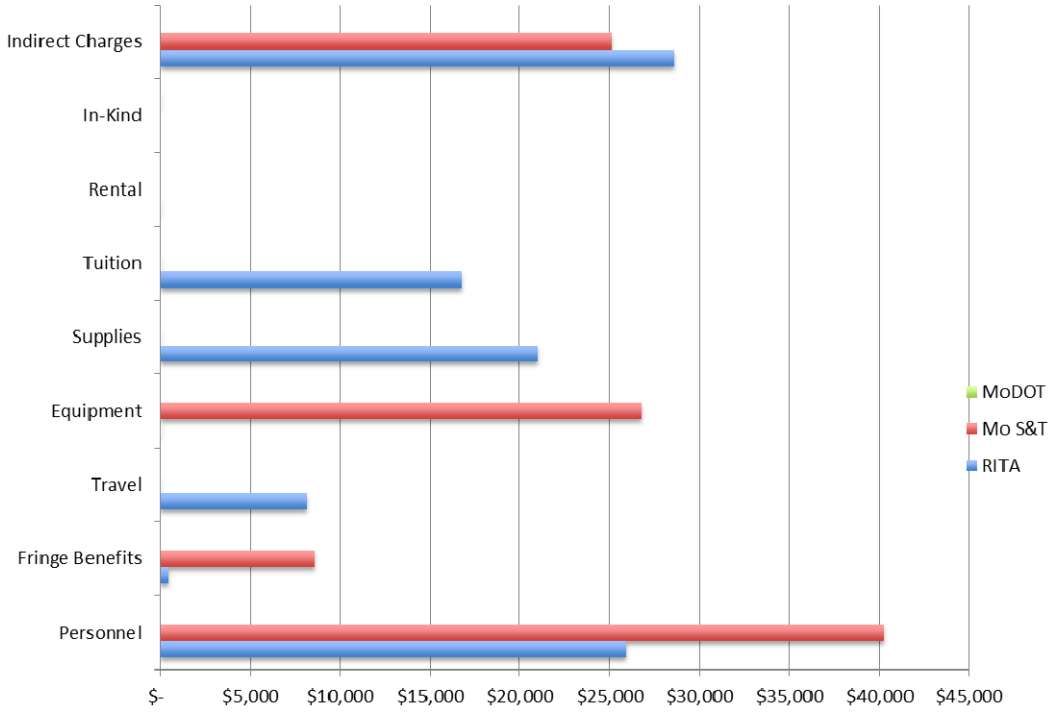

Fig. 27 Cummulative expenditures by sponsor